Skelemin Association with $\alpha_{IIb}\beta_3$ Integrin: A Structural Model

Vitaliy Gorbatyuk[1], Khiem Nguyen[1], Nataly P. Podolnikova[2], Lalit Deshmukh[+1], Xiaochen Lin[1], Tatiana P. Ugarova[2] and Olga Vinogradova[*1]

[1]Department of Pharmaceutical Sciences, School of Pharmacy, University of Connecticut at Storrs, Storrs, CT 06269 [2]Center for Metabolic and Vascular Biology, School of Life Sciences, Arizona State University, Tempe, Arizona 85287

Running head: integrin-skelemin interaction

Funding Source statement:

This work was supported in parts by AHA 0855768D to O.V., AHA 0835257N to N.P.P and NIH HL 63199 to T.P.U.

*Address correspondence to: Olga Vinogradova, Department of Pharmaceutical Sciences, 69 North Eagleville Rd, Unit 3092, Storrs, CT 06269-3092, Phone: (860) 486-2972, Fax: (860) 486-6857, E-mail: olga.vinogradova@uconn.edu

[+]Current address: Laboratory of Chemical Physics, National Institute of Diabetes and Digestive and Kidney Diseases, NIH, Bethesda, MD 20892-0520

Abbreviations

$C_{12}E_5$, pentaethylene glycol monododecyl ether; DTT, dithiothreitol; ECM, extracellular matrix; FA, focal adhesions; FN, fibronectin; FX, focal complex; IgC2, immunoglobulin C2-like domain; ITC, isothermal titration calorimetry; m-PROXYL, 3-maleimido-PROXYL; NMR, nuclear magnetic resonance spectroscopy; NOE, nuclear overhauser effect; PMSF, phenylmethanesufonyl fluoride; PRE, paramagnetic relaxation enhancement; RDC, residual dipole coupling; SOS, sodium octyl sulfate; Tris, Tris(hydroxymethyl)aminomenthane; trNOE, transferred nuclear overhauser effect.

Abstract

Over the last two decades, our knowledge concerning intracellular events that regulate integrin's affinity to their soluble ligands has significantly improved. However, the mechanism of adhesion-induced integrin clustering and development of focal complexes, which could further mature to form focal adhesions, still remains under-investigated. Here we present a structural model of tandem IgC2 domains of skelemin in complex with the cytoplasmic tails of integrin $\alpha_{IIb}\beta_3$. The model is generated based upon NMR data and this tertiary assembly illuminates a potential link between the essential cell adhesion receptors and myosin filaments. This connection may serve as a basis for generating the mechanical forces necessary for cell migration and remodeling.

In order for multicellular organisms to survive, individual cells must adhere to each other and to their extracellular surrounding. This adhesion is primarily mediated by integrins (*1*), a family of transmembrane glycoprotein heterodimers. Integrins connect the extracellular matrix (ECM) and the cytoskeleton within the cells through numerous interactions with their cytoplasmic targets. Integrins also function as bidirectional signal transducers (*2*) and may serve as sensors of ever-changing mechanical forces (*3*). It has been shown that integrins bind to ECM proteins via their extracellular domains, which triggers conformational changes and clustering of integrins. This clustering initially forms a small network called motility-inducing focal complexes (FXs), which could be ultimately replaced in fully spread cells by large intracellular complexes of variable content known as focal adhesions (FAs) (*4*).

Skelemin, also known as myomesin-1.1 and originally identified as a muscle M-line cytoskeletal protein of 185 kDa, is expressed primarily in embryonic heart (*5*) and has been shown to play a critical role in mediating the connection between ECM and cytoskeleton during the early stages of cell spreading (*6*). It belongs to a family of cytoskeletal proteins, all associated with myosin thick filaments in skeletal and cardiac muscles, and contains a unique N-terminal myosin-binding domain, five fibronectin (FN) type III-like domains, six immunoglobulin C2-like (IgC2) domains, and a C-terminal immunoglobulin domain involved in homo-dimerization (*7*). Its major isoform (myomesin-1.2) is shorter by about a hundred residues, which are spliced out between FN domains 2 and 3. Skelemin is localized to FXs, but not FAs, through the direct interaction of its IgC2 domains 4 and 5 with β_3-integrin cytoplasmic tail (*8*). The second major member of this family, myomesin-2, is a product of myomesin 2 gene with a shorter N-terminus, resulting in molecular weight of about 165 kDa, and has about 71% homology with skelemin. It is expressed in diverse non-muscle tissues including CHO cells, platelets and endothelial cells (*8, 9*).

We and the others have shown that skelemin is one of the rare proteins that can bind both β and α subunit of integrin receptors (*10, 11*). Although skelemin cannot activate integrins, it has been suggested that skelemin exerts contractile force and modulates the attachment of cytoskeletal proteins and Src to integrin clusters during early stages of cell spreading (*12*). A recent study (*13*) has unveiled the ability of skelemin filaments to be stretched to about 2.5-fold its original length by reversible unfolding of the linkers connecting Ig domains. Pinotsis and co-workers have employed a combination of four complementary structural biology methods to investigate how the repetitive structure of skelemin contributes to muscle elasticity. This work explained, for the first time, skelemin's capability to act as a highly elastic ribbon for maintaining the overall structural organization of the sarcomeric M-band of skeletal muscle.

In the present work, we investigated how two skelemin repeats are organized and may contribute to its unique elastic properties in non-muscle cells. Knowledge of these details is particularly important considering the role of skelemin as a connector between cell surface receptors and the cytoskeleton. We previously determined the solution structure of skelemin immoglobulin domain 4 (Sk4), modeled domain 5 (Sk5), and investigated how major platelet integrin $\alpha_{IIb}\beta_3$ binds to Sk45 (*11*). Here, we examined skelemin tandem IgC2 domains 4 and 5 (hereafter addressed as Sk45) together with their inter-connecting linker using solution Nuclear Magnetic Resonance (NMR) Spectroscopy. We present the structure of Sk45 and the docking model of its tertiary complex with $\alpha_{IIb}\beta_3$ integrin cytoplasmic tails. We also investigated thermodynamic profiles of skelemin interactions with integrin cytoplasmic tails by Isothermal Titration Calorimetry (ITC). Overall, the docking model supports the role of skelemin in stabilizing integrin activated, clustered state through the simultaneous binding to its two separated cytoplasmic tails.

Experimental Procedures

Expression and Purification, Peptides and Cells

The cloning of mouse Sk4 and Sk45 has been described previously (*11*). Single-site mutagenesis of Sk45, converting solvent exposed C^{1354} to S (to improve solubility of recombinant construct) and C-terminal K^{1424} to C (to introduce paramagnetic spin label), was performed using the QuikChange kit (Agilent Technologies). The mutant plasmids were transformed into Rosetta (DE3) competent cells (EMD Millipore). Protein expression was carried out using LB or M9 minimal media with $^{15}NH_4Cl$, and/or ^{13}C-glucose as the sole nitrogen and carbon sources, at 37 ^{o}C. Cultures were induced with 1 mM ITPG at an OD_{600} of ~ 0.6. The cells were harvested 4 hours after induction. For Sk4, Sk45 (construct with C^{1354}S mutation), and Sk45m (construct with both C^{1354}S and K^{1424}C mutations), cells were resuspended in a buffer containing 20 mM Tris, pH 8, 300 mM NaCl, 10 mM imidazole, 1 mM DTT, 1 mM PMSF, 1 tablet of complete protease inhibitor cocktail (Roche Applied Science). The suspension was lysed by passage through French press (Thermo Electron). The supernatant fractions were loaded onto Ni-NTA agarose resin (Qiagen) and proteins were eluted with a buffer containing 20 mM Tris, pH 7.5, 300 mM NaCl and 500 mM imidazole. To cleave the His-tag, thrombin was added directly to the Ni-NTA column. Cleavage was done in a 37 ^{o}C incubator for 4 hours with periodic mixing (50 mM Tris, 150 mM NaCl, 1 mM EDTA, pH 7.5). Thrombin was inhibited by the addition of equivalent amounts of PMSF. The eluate was further purified by size exclusion chromatography (16/60 Superdex 75 column, GE Healthcare) in 50 mM NaCl, 20 mM KPO_4, pH 6.8.

Peptides, corresponding to the integrin cytoplasmic tails, were synthesized chemically (NEOpeptides): α_{IIb} (starting from W^{988}), N-terminus of β_3 (K^{716}-W^{739}), and C-terminus of β_3 (K^{738}-T^{762}). Myristoylated peptides, corresponding to skelemin's sequence, were synthesized by Peptide 2.0 (Chantilly, VA): ^{1369}THIVWYKDEREISVDEKHD^{1387} and ^{1377}EREISAAAKHD^{1387}, which is a triple mutant (VDE→AAA).

Human fibrinogen was obtained from Enzyme Research Laboratories (South Bend, IN). CHO cells expressing $\alpha_{IIb}\beta_3$ were described previously (*14*) and were maintained in Dulbecco's modified Eagle's medium/F-12 medium supplemented with 10% fetal bovine serum and 25 mM HEPES.

NMR Spectroscopy

NMR experiments were performed on uniformly ^{15}N/^{13}C-labeled samples (unless stated otherwise) prepared in buffer containing 20 mM KPO_4, pH 6.8, and 7% D_2O. Spectra were recorded at 25 °C on a Varian INOVA 600 MHz spectrometer equipped with a cold probe. The standard BioPack pulse sequences were used. Spectra were processed using NMRPipe (*15*) and analyzed with CCPN Analysis (*16*).

The backbone resonance assignments for Sk45 were obtained from the set of triple resonance experiments, HNCO, HN(CA)CO, HNCA, HNCACB, CBCA(CO)NH and HBHA(CO)NH. Due to a very high degeneracy of the peaks in HCCH-COSY and HCCH-TOCSY spectra and very weak C(CO)NH and H(CCO)NH spectra, only a partial assignment of the side chain resonances was achieved from these data. The Sk45 tandem is very rich in methyl-containing residues, which constitute 32% of the protein sequence. Since methyl groups form the core of a protein and, thus, could provide very valuable distance restrains for the structure calculation, we collected methyl-optimized (H)CCmHm-TOCSY experiment from the BioPack library. From this spectrum, we were able to obtain the chemical shift assignment for all methyl groups and this information turned to be crucial for the convergence of the structure calculation. In total, chemical shift assignment was obtained for 80% of protons, 41% of carbons and 71% of nitrogens.

$^{1}D_{HN}$ residual dipolar couplings (RDC) were derived from the difference between peaks positions in ^{1}H-^{15}N HSQC and TROSY spectra recorded in isotropic and anisotropic conditions. Three different alignment media were used: Pf1 phage (ASLA Biotech), mixture of

$C_{12}E_5$/hexanol, or $C_{12}E_5$/hexanol/sodium octyl sulfate (Sigma-Aldrich, C12E15 concentration was 4.1%, C12E5:SOS=30:1 molar ratio). In all media, the His-tag of Sk45 was cleaved prior to collecting RDCs. A data set for Sk45 with the His-tag intact was also collected in Pf1 phage solution.

Paramagnetic relaxation enhancement (PRE) experiments were performed with Sk45m, where the solvent exposed K^{1424} was mutated to cysteine. The ^1H-^{15}N HSQC spectra were collected with and without 3-maleimido-PROXYL (m-PROXYL) spin label. The effect of the spin label on the signal intensities was estimated from the normalized intensity differences in the spectra with and without the spin label.

Transferred NOEs (trNOE) for α_{IIb} cytoplasmic tail in complex with Sk45 were obtained at the peptide to protein ratio of 100:1 with the mixing time of 400 msec as previously mentioned (*11*). The ^1H assignments for α_{IIb} were performed previously (*17*).

The titrations of α_{IIb} or β_3 into the Sk45 solution were monitored with ^1H-^{15}N HSQC spectra at the peptide to protein ratios varied from 1:1 to 5:1.

Structures Calculation

The Sk45 structure calculation and NOE assignment was carried out with ARIA 2.3 (*18*) and Xplor-NIH (version 2.33). The unassigned NOEs from 3D ^{15}N-NOESY and ^{13}C-NOESY experiments along with dihedral angle constraints were used as an input for ARIA. The dihedral angles were predicted with DANGLE in CCPN Analysis (*16*). In the subsequent calculations, hydrogen bond constraints were introduced. The characteristic NOE pattern, the CSI secondary structure prediction, and H-D exchange data gave rise to 156 constraints (two constraints per H-bond). In some cases, hydrogen bond constraints were set to have multiple partners. Later, the obtained ARIA NOE assignments were manually verified in CCPN Analysis. Stereospecific assignment of prochiral groups was achieved using a floating assignment approach as implemented in ARIA.

The structure was further refined with RDCs using Xplor-NIH. Initially, the two domains were refined with RDCs independently. For this, the sets of $^1D_{HN}$ RDCs for the three media were divided in the two parts: one for each skelemin domain. In addition to RDC restraints, the calculation was supplied with ARIA-derived distance constraints, dihedral and H-bond restraints. In the next step, the two domains were treated as rigid bodies connected by a flexible linker and RDCs were used to orient the domains. This time, every set of RDC restraints for the three different media was used as a whole, containing RDCs for the both domains. A total of 1000 structures were calculated in the “rigid body” run and the lowest energy 20 structures were further refined in water with Xplor-NIH. In the water refinement step, all experimental constraints were used, including NOEs, dihedral, H-bond, and RDC restraints. These 20 refined structures were chosen as a representative ensemble.

The α_{IIb} peptide structure in the complex with Sk45 was obtained based upon trNOE restraints using ARIA and the ensemble of 20 structures with minimal overall energy was refined in explicit water.

During the course of the calculations, the quality of the molecular structures was assessed with ARIA/CNS built-in scripts and PROCHECK-NMR (*19*).

Modeling

The HADDOCK webserver (*20*) was used for docking of α_{IIb} and β_3 integrin tails to Sk45. For α_{IIb}/Sk45 binary complex determination, the best NMR structures of α_{IIb} and Sk45 from the NMR ensembles were chosen. During the docking, the following residues were set as active: 990, 992-997 of α_{IIb} and 1361, 1363, 1394 of Sk45. For β_3 docking, we have used the first representative of the ensemble with PDB ID 1M80. The active residues for this docking were 716, 722, 724, and 725 of β_3 and 1368, 1370, 1372, 1374, 1382, 1383, and 1411 of Sk45. The flexible unstructured N-terminal residues (1207 to 1225) of Sk45 were removed before docking.

Electrostatic Potential

The electrostatic potential of Sk45 was calculated using Adaptive Poisson-Boltzmann Solver (APBS) (*21*). The pdb file of Sk45 was uploaded to the pdb2pqr webserver (*22*) using PARSE as the forcefield and PROPKA to assign protonation states. The output files were used to create the electrostatic potential map by APBS. The electrostatic potential map was visualized by UCSF Chimera (*23*) using the built-in electrostatic surface coloring module.

ITC

Isothermal Titration Calorimetry was performed on a low volume Nano ITC (TA Instruments). Peptides corresponding to integrin cytoplasmic tails were solubilized in the buffer 50mM NaCl, 20mM KPO_4, and pH 6.8. All ITC experiments were performed at 25^{O}C, 300 rpm mixing, 300 seconds time intervals between injections, and 3Sl injection volumes. The concentrations used are as follows: 2.5 mM C-terminal β_3 and 0.175 mM Sk4, 1.3 mM N-terminal β_3 and 0.177 mM Sk45, and 1.9 mM α_{IIb} and 0.177 mM Sk45. The analysis of the data was done in NanoAnalyze Software (TA Instruments) suite using “Independent” model.

Adhesion Assays

The wells of 96-well tissue culture plates (Immulon 4B) were coated with the 2.5 Sg/ml of fibrinogen overnight at 4 °C. The wells were post-coated with 1% BSA. Cells were labeled with 10 μM Calcein AM (Molecular Probes, Eugene, OR) for 30 min at 37°C, washed and resuspended in DMEM/F-12 medium at 1×10^{5} cells/ml. Cells were mixed with different concentrations of peptides for 20 min at 22 °C before they were added to the wells coated with adhesive substrates. Aliquots (100 μl) of cells were added to the wells and incubated at 37°C for 30 min. The nonadherent cells were removed by two washes with phosphate-buffered saline (PBS), and fluorescence was measured in a fluorescence plate reader (Applied Biosystems, Framingham, MA). The number of adherent cells was determined using the fluorescence of aliquots with a known number of labeled cells.

RESULTS

Structure of Skelemin Tandem Sk45

Skelemin IgC domains 4 and 5 have been shown to interact with β_3 cytoplasmic tail (*9*). We have determined, by solution NMR, that a single domain Sk4 adopts a very well-known IgC2-fold containing seven β-strands in two β-sheets forming a β-sandwich (*11*). However, poor behavior of skelemin domain 5 in the solution has precluded its detailed structural characterization by NMR. To avoid this problem, and to improve the solubility of the tandem Sk45, we have mutated the surface exposed C^{1354} of domain 5 to serine in order to obtain a 27 kDa protein construct suitable for solution NMR studies.

The complete backbone and partial side chain resonance assignments were found sufficient for *ab-initio* structure calculation of the domains fold via the classical NOE-based approach supported by RDC data. A total of 2647 NOE constraints, 351 RDC, 156 H-bond, and 311 backbone dihedral restraints, allowed us to obtain the folds with RMSD 0.97 Å for Sk4 domain (the well-ordered residues 1227- 1327 are used for superimposition) and 1.37 Å for Sk5 domain (the well-ordered residues 1344-1380 and 1391-1427). As expected, the tandem domains 4 and 5 adopted a well-known IgC2-fold and contained seven β-strands in two β-sheets forming two β-sandwiches connected through a partially helical linker. Figure 1A and B present 20 structures with the lowest target energy functions. These structures were obtained from the calculations where RDCs were divided in the two separate sets (one for each domain), effectively treating

the two domains as independent entities. The RDC fits for this calculation show an impeccable correlation within the individual domains (Figure 2A). However, the correlation is poor for the tandem (Figure 2B), reflecting the fact that the mutual orientation of the domains in these structures are not optimized.

Thus, the observed NOEs alone were insufficient for restricting the domains connected in the tandem through a loosely structured helical linker. Therefore, in order to define the mutual orientation of domains 4 and 5, we obtained and utilized long range data, such as RDCs and PRE. As a rule, the RDC approach is based on the notion that when a multi-domain molecule with no or little relative inter-domain motion is settled within an anisotropic environment, the environment does not change the mutual domain orientation. In turn, this implies that the alignment tensors for each domain and for the entire molecule in the anisotropic environment are equal. Thus, for orienting the domains within the multi-domain molecule by means of RDCs, the order tensors of the domains have to be made collinear. However, an inherent degeneracy exists since residual dipolar coupling constants can be satisfied by tensors which differ by 180° around the tensor axes. To resolve this ambiguity, data from several types of alignment media are used simultaneously during structure calculations (*24*).

We have used the "rigid body" approach for the domain orientation in the Sk45 tandem. The starting structures had the domains refined with all experimental constraints as described above. In the "rigid body" Xplor-NIH run, we calculated 1000 structures in order to sample the entire conformational space and we used RDC constraints as a single set for every alignment medium, which would treat the tandem as a whole. The final ensemble of the 20 lowest energy structures has RMSD 3.1 Å over residues 1227-1327 (domain 4) and 1344-1427 (domain 5) and is presented in Figure 3A. In order to lift the four fold degeneracy, the alignment media should produce non-collinear order tensors. The orientation of the tensors that we obtained for the four sets of RDCs differs by up to 45° (Figure 3B). $^{1}D_{HN}$ RDCs fits for both domains within Sk45 structure and are presented in Figure 3C. The quality of these fits is excellent, as justified by the correlation coefficients of 0.96, 1.00, 1.00, and 0.99 for Sk45 with His-tag in Pf1, Sk45 without His-tag in Pf1, C12E5/hexanol, and C12E5/hexanol/SOS anisotropic media, respectively. Thus, we were able to find the inter-domains orientation. This ensemble has been deposited to Protein Data Bank (access code XXX). Statistics of this ensemble are presented in Table 1.

The obtained domain orientation coincides with PRE data, where the paramagnetic spin label, 3-maleimido-PROXYL (m-PROXYL), is introduced to the solvent-exposed C-terminal cysteine $K^{1424}C$ of the domain 5. The HSQC spectrum of Sk45 $K^{1424}C$ mutant resembles the spectrum of Sk45 with a difference only near the mutation site. Thus, we can conclude that the molecular Ig-fold is preserved in this mutant. Upon attaching the m-PROXYL spin label to the protein, we have observed sequence specific ^{1}H-^{15}N HSQC signal agitations. The peaks, which are the most significantly deteriorated by the relaxation enhancement, all belong to the residues located in the domain 5: 1376, 1377, 1404, 1406, 1407, 1408, 1422, 1423, 1424, and 1425. As it is seen from the NMR structure (Figure 1C), all these residues (shown in red) are in close proximity to the introduced cysteine residue at the position 1424 (depicted with the thicker bonds).

The comparison of the ^{1}H-^{15}N HSQC spectra of Sk4 and Sk45 constructs revealed residues that experienced shifts in resonance frequencies due to the addition of the domain 5. As expected, the most disturbed are Sk4 C-terminal residues 1322-1329, which belong to the helical linker in Sk45. The other affected Sk4 residues are 1234-1242, 1273, 1287-1295, and 1315-1319. These regions in the presented NMR structure (Figure 1D, displayed with thicker bonds) are also in close proximity to the C-terminal helix of Sk4 construct. Thus, PRE and chemical shift perturbation data confirm that the two domains are rather distant in space and no inter-domain interaction in the Sk45 tandem is observed.

Interaction of Sk45 with Cytoplasmic Tails of $\alpha_{IIb}\beta_3$ Integrin

Previously, we defined skelemin binding surface on platelet integrin $\alpha_{IIb}\beta_3$ and demonstrated that this interaction is consistent with an attenuated inter-subunit clasp (*11*). To address the mechanism of this interaction, and to define the thermodynamic forces driving the process, we have employed ITC. We used Sk4 and Sk45 constructs titrated with either full length α_{IIb} cytoplasmic tail (Figure 4A, Figure S1.B) or short synthetic peptides corresponding to β_3 N- or C-termini (Figure S1.A), as previously described (*11*). The results, summarized in Table 2, revealed very weak interactions which were in the tens SM range. These reactions were predominantly driven by entropy. For all cases, the stoichiometry of interactions was found to be one.

Because the interaction of α_{IIb} with skelemin is weak with fast off-rate, we were able to perform the transferred NOE experiments on α_{IIb}/Sk45 solution. With trNOE constraints supplied to ARIA, we calculated the structure of the bound peptide. Upon binding, the peptide adopts a U-shaped structure (ensemble depicted in Figure 4B). From the HSQC titration experiments, we found that residues 1361, 1363, and 1394 form the binding site for α_{IIb} on the Sk45 surface. The best NMR structures of α_{IIb} and Sk45 were used for *in silica* docking with HADDOCK software. After the docking of 1000 structures, the best 200 models were refined in water and among them the 5 clusters were identified by HADDOCK. The largest cluster with the lowest score had 114 models with RMSD 4.1 Å from the over-all lowest energy model.

We performed trNOE experiments for the short synthetic β_3 peptides earlier and found a very limited number of additional peaks, preventing us from determining the structure of the bound β_3 ensemble (*11*). Here, we studied β_3 interaction with Sk45 by HSQC titration experiments performed on the ^{15}N-labeled Sk45 sample. In these experiments, we were unable to observe any reliable chemical shift perturbations in titration with C-terminal β_3 peptide, most probably due to the repelling effect of the flexible unstructured N-terminus of Sk45. However, we observed concentration dependent chemical shifts (Figure 4C, Figure S2) and found that residues 1368, 1370, 1372, 1374, 1382-1384, and 1411 of Sk45 are affected by N-terminal β_3 peptide binding. These residues were used for *in silica* docking of the β_3 conformer (PDB ID 1M80) into the NMR structure of Sk45 presented here. The best HADDOCK cluster contained 17 models with RMSD 0.9 Å from the over-all lowest energy model.

The combined docking model of Sk45 tertiary complex with integrin cytoplasmic tails is presented in Figure 5 and discussed below. The data used to generate the model is summarized in Table S1.

To prove the relevance of the generated model interface *in vivo,* and to further assess the role of the identified binding site for the integrin $\alpha_{IIb}\beta_3$, we synthesized the peptide THIVWYKDEREISVDEKHD, and tested the effect of this peptide on the adhesion of CHO cells expressing $\alpha_{IIb}\beta_3$ to immobilized fibrinogen. This peptide represents the two full length β–strands of the domain 5 β–sandwich of skelemin that come into contact with the membrane-proximal region of β_3 integrin, according to our model. This peptide was considered to be stable enough to maintain a hair-pin sort of structure through the internal hydrogen bonds in the absence of the rest β–strands. Increasing the concentration of the peptide progressively blocked cell adhesion in dose-dependent manner, where the IC_{50} was determined to be 33 SM as shown in Figure 4D. The inhibition was specific as the control peptide, in which VDE residues were mutated to AAA, did not appear to have any effect on cell adhesion.

DISCUSSION

As a family of major cell adhesion receptors, integrins uniquely combine bi-directional signaling capabilities with the structural functions of linking extracellular matrix proteins to the cytoskeleton. With a myriad of potential intracellular targets, all these functions could be accomplished only through spatially and temporally controlled interactions. We have

investigated how major platelet integrin, $\alpha_{IIb}\beta_3$, binds to skelemin, a cytoskeletal protein found in non-muscle cell focal complexes during the earlier phases of cell spreading.

We solved the NMR structure of the skelemin tandem domains with the help of RDC data from the four alignment media for orienting the Sk45 two domains in a solution with the "rigid body" approach. Figure 3A depicts the superposition of the representative ensemble of Sk45 NMR structures with the X-ray structure of human myomesin-1 for comparison (PDB ID 3RBS, shown in violet with thicker bonds) (*13*). We have back-calculated the RDCs for the crystal structure of the myomesin-1 domains 10 and 11 and found no correlation with RDCs set for the Pf1 medium (with 0.69 correlation coefficient of this fit) as well as a rather poor correlation (correlation coefficient of 0.93 in comparison to 1.00 of NMR ensemble) for the C12E5/hexanol alignment medium (Figure 3D), suggesting a notable deviation from the ensemble in the solution. Not surprisingly, the major differences were found within the linker connecting domains 4 and 5 (shown zoomed in the insert of Figure 3A with Sk4 domain used for superimposition). While the X-ray structure suggests the presence of well-defined straight helix through-out this region, this is not the case in this solution. We observed that only the N-terminal half of the linker, connected to domain 4, forms a regular α-helix. The second C-terminal half of the linker was quite loose, with a number of NMR resonances broadened out due to conformational heterogeneity and no evidence for regular α-helical characteristic (i, i+3) connections in NOESY spectra. There is also a noticeable difference in the angle between the helix formed and the β-strand to which it is attached. Thus, we conclude that in solution the linker connecting two domains is much more flexible and dynamic so that it could be deduced from the crystal structure. As the linkers between individual Ig domains may serve as springs, conferring the elasticity to the skelemin/target proteins assemblies, or as sensors of mechanical forces applied across the membrane, this particular finding is important for defining mechanical properties in integrin signaling. The N-terminal half of the linker is stabilized by the interactions with domain 4 as we observed in HSQC spectra. This coincides with finding that Ig domain/helix interface area is structurally conserved throughout other Ig tandem domains of myomesin-1 (*13*). Limited flexibility of inter-Ig domains arrangements, suggested from multiple crystal structures, is not exactly limited in solution with the loose C-terminal half of the linker and noticeable difference in the angle between the linker and domain 4 (see the inset in Figure 3A).

The interaction of skelemin with integrin α_{IIb} and β_3 cytoplasmic tails was found to be very weak. In our ITC studies, the measured K_d values were all above 10SM (Table 2). Interestingly, this interaction was driven mainly by entropy since the enthalpy contribution was measured to be very small. The present data confirmed our previous findings (*11*), suggesting that i) the skelemin/integrin interactions are not very stable, which is an important feature allowing dynamic regulation of cell spreading process, and ii) multiple interactions might be required to mediate physiologically significant responses favoring the involvement of integrin clustering.

In addition, our HSQC titration experiments indicated that the α and β binding interfaces on skelemin surface do not overlap, but are located on the opposite sides of the domain 5, rendering the possibility of competitive binding very unlikely. Due to the weakness of skelemin/integrin interactions described above, it was not possible to conjur a high resolution structure of the tertiary complex. Instead, we have docked Sk45 with integrin α_{IIb} and β_3 cytoplasmic tails utilizing HADDOCK. The docking was directed by the restraints acquired through chemical shifts mapping, trNOE NMR experiments, and published mutagenesis data (*10, 12*). Figure 5 demonstrates the model of integrin/skelemin tertiary complex and its potential placement with respect to the lipid bilayer.

The mode of integrin interaction with skelemin is quite different between the two subunits, as can be deduced from the binding interface between IgC-2 like domains 4-5 and $\alpha_{IIb}\beta_3$ cytoplasmic tails. For α_{IIb} subunit, a number of van der-Waals interactions bring it into skelemin IgC5's predominantly hydrophobic binding pocket, with the major interactions arising from α_{IIb} F^{992} and F^{993} side chains found in close proximity to I^{1392} and the side chain of α_{IIb} W^{988} making

hydrophobic contacts with F^{1388}, K^{1389}, and, possibly, D^{1387} of IgC5. Additionally, a hydrogen bond is formed between K^{994} amine of α_{IIb} and the backbone oxygen of A^{1343}.

In contrast, binary β_3/skelemin interface is mostly based upon a network of hydrogen bonds between β_3 N-terminus and skelemin IgC5, including the linker. N-terminal K^{716} of β_3 forms hydrogen bonds with the side chain of E^{1384}, while K^{725} hydrogen bonds with the backbone oxygen of D^{1415}. There also are hydrophobic interactions between β_3 H^{722} as well as the side chain carbons of Sk45 K^{1413} and E^{1368}. From the skelemin side, IgC5 K^{1418} forms an extensive hydrogen bonding network, which includes β_3 residues D^{723}, through both the side chain and backbone oxygen, and E^{726}, through the side chain only. Our in-cell adhesion assay has further confirmed the proposed arrangement (Figure 4D). Among these residues, K^{716}, H^{722}, and K^{725} have been previously identified as critical for interaction with the skelemin IgC-2 like domains 3-7 using synthetic peptides corresponding to the membrane-proximal part of the β_3 cytoplasmic tail. In addition, α_{IIb} F^{992} was shown to interact with skelemin (*10*). The electrostatic surface potential of the zoomed IgC5 region presented in Figure 5B helps to visualize a mostly hydrophobic cleft on the left interacting with α_{IIb} subunit and predominantly negatively charged binding site for β_3 subunit on the right. Two hydrogen bonds are found within skelemin linker helix: the side chain nitrogen of K^{1321} is connected to β_3 N^{744} while E^{1328} oxygen interacts with the side chain amine of R^{736}. Because we have not observed the chemical shift perturbations for domain 4 in our titration experiments, no restraints linking β_3 C-terminus to IgC4 were introduced during the HADDOCK docking. Not surprisingly, the model demonstrates no major interactions between IgC4 and β_3, with only a couple of hydrophobic contacts found between side chains of IgC4 residues E^{1293} and N^{1294} and β_3 A^{750}.

Previously, we structurally characterized $\alpha_{IIb}\beta_3$ cytoplasmic heterodimer, which plays an important role in maintaining integrin in its latent state (*17*). Superimposition of our tertiary model with $\alpha_{IIb}\beta_3$ heterodimer reveals steric clashes, making it extremely difficult, if not impossible, for both the subunits to interact with skelemin in the presence of inter-subunit clasp. Since some of the α_{IIb} and β_3 residues critical for skelemin binding ($\alpha_{IIb}F^{922}$ and β_3H^{722}) are also involved in the formation of the $\alpha_{IIb}\beta_3$ clasp (*17*), it appears that unclasping of the tails is prerequisite for skelemin binding. Although we have previously demonstrated that $\alpha_{IIb}\beta_3$ does not interact with skelemin in resting platelets, it is recruited to the receptor during platelet adhesion and upon activation with agonists. Considering the fact that cytoplasmic tails of $\alpha_{IIb}\beta_3$ have a higher mutual affinity (of 5.7 SM as measured by ITC, Figure S1.C) than any single subunit to skelemin (Table 2), this observation supports the notion that skelemin is not an integrin activator, and rather serves as a modulator of integrin attachment to Src or cytoskeleton.

In Figure 5C, we have positioned the tertiary complex with respect to the lipid bilayer. As presented, skelemin Ig domains 4 and 5 may be placed parallel to the membrane surface. With this arrangement, α_{IIb} subunit comes out of the membrane almost perpendicularly with its W^{988} side chain making contacts with lipid head-groups at the membrane-cytoplasm interface. Integrin β_3 subunit, on other hand, is arranged at a sharp acute angle with its K^{716} side chain making contacts with negatively charged patch on the surface of IgC5 which sticks out as being repelled by negatively charged inner leaflet of the lipid bilayer. In the inset of Figure 5C, we have also marked IgC5 positively charged residues, which potentially may interact with negatively charged lipids. The rest of IgC5 negative patch is arranged to interact with either the 6^{th} IgC-2 like domain of skelemin or with any other potential target having positively charged solvent exposed surface.

To conclude, we have determined a three dimensional structure of tandem IgC2-like domains 4 and 5 of skelemin, connected through a stretchable helix-containing linker, by NMR. This linker region was found to be restrained enough to define the mutual orientation of the two domains tumbling as a single unit in solution, although it is less more dynamic than suggested by earlier X-ray studies of the human homolog myomesin-1. We have shown that interaction

between skelemin and integrin cytoplasmic domain is weak and predominantly entropy driven. This is consistent with the findings that skelemin is unable to activate the receptors. We have built a tertiary model of $\alpha_{IIb}\beta_3$ integrin cytoplasmic tails complexed with the tandem domains and validated it with cellular adhesion assays. While some of the interactions between K^{716} side chain of β_3 tail and skelemin may occur in the presence of α_{IIb} subunit still bound to β_3, disruption of membrane-proximal α/β clasp and release of α_{IIb} F^{992} and β_3 $H^{722}/D^{723}/E^{726}$ side chains is necessary for α_{IIb} to bind to skelemin and for β_3 to stabilize its interface with skelemin. Thus, our model favors skelemin role as a stabilizer for the activated integrins and integrin clusters by connecting α and β subunits from adjacent receptors.

Acknowledgements

We would like to thank Drs. Sergiy Tyukhtenko from North Eastern University, Mark Maciejewski from University of Connecticut Health Center and G.T.V. Swapna from Rutgers University for their help with data acquisition at high field NMR spectrometers. The WeNMR project (European FP7 e-Infrastructure grant, contract no. 261572, www.wenmr.eu), supported by the European Grid Initiative (EGI) through the national GRID Initiatives of Belgium, France, Italy, Germany, the Netherlands, Poland, Portugal, Spain, UK, South Africa, Malaysia, Taiwan, the Latin America GRID infrastructure via the Gisela project and the US Open Science Grid (OSG) are acknowledged for the use of web portals, computing and storage facilities.

References

1. Hynes, R. O. (1992) Integrins: versatility, modulation, and signaling in cell adhesion, *Cell 69*, 11-25.
2. Hynes, R. O. (2002) Integrins: bidirectional, allosteric signaling machines, *Cell 110*, 673-687.
3. Geiger, B., and Bershadsky, A. (2001) Assembly and mechanosensory function of focal contacts, *Curr Opin Cell Biol 13*, 584-592.
4. Webb, D. J., Parsons, J. T., and Horwitz, A. F. (2002) Adhesion assembly, disassembly and turnover in migrating cells -- over and over and over again, *Nature cell biology 4*, E97-100.
5. Steiner, F., Weber, K., and Furst, D. O. (1999) M band proteins myomesin and skelemin are encoded by the same gene: analysis of its organization and expression, *Genomics 56*, 78-89.
6. Price, M. G., and Gomer, R. H. (1993) Skelemin, a cytoskeletal M-disc periphery protein, contains motifs of adhesion/recognition and intermediate filament proteins, *J Biol Chem 268*, 21800-21810.
7. Pinotsis, N., Lange, S., Perriard, J. C., Svergun, D. I., and Wilmanns, M. (2008) Molecular basis of the C-terminal tail-to-tail assembly of the sarcomeric filament protein myomesin, *EMBO J 27*, 253-264.
8. Reddy, K. B., Bialkowska, K., and Fox, J. E. (2001) Dynamic modulation of cytoskeletal proteins linking integrins to signaling complexes in spreading cells. Role of skelemin in initial integrin-induced spreading, *J Biol Chem 276*, 28300-28308.
9. Reddy, K. B., Gascard, P., Price, M. G., Negrescu, E. V., and Fox, J. E. (1998) Identification of an interaction between the m-band protein skelemin and beta-integrin subunits. Colocalization of a skelemin-like protein with beta1- and beta3-integrins in non-muscle cells, *J Biol Chem 273*, 35039-35047.
10. Podolnikova, N. P., O'Toole, T. E., Haas, T. A., Lam, S. C., Fox, J. E., and Ugarova, T. P. (2009) Adhesion-induced unclasping of cytoplasmic tails of integrin alpha(IIb)beta3, *Biochemistry 48*, 617-629.

11. Deshmukh, L., Tyukhtenko, S., Liu, J., Fox, J. E., Qin, J., and Vinogradova, O. (2007) Structural insight into the interaction between platelet integrin alphaIIbbeta3 and cytoskeletal protein skelemin, *J Biol Chem 282*, 32349-32356.
12. Li, X., Liu, Y., and Haas, T. A. (2013) Skelemin in integrin alpha(IIb)beta(3) mediated cell spreading, *Biochemistry 52*, 681-689.
13. Pinotsis, N., Chatziefthimiou, S. D., Berkemeier, F., Beuron, F., Mavridis, I. M., Konarev, P. V., Svergun, D. I., Morris, E., Rief, M., and Wilmanns, M. (2012) Superhelical architecture of the myosin filament-linking protein myomesin with unusual elastic properties, *PLoS biology 10*, e1001261.
14. Podolnikova, N. P., Yakubenko, V. P., Volkov, G. L., Plow, E. F., and Ugarova, T. P. (2003) Identification of a novel binding site for platelet integrins alpha IIb beta 3 (GPIIbIIIa) and alpha 5 beta 1 in the gamma C-domain of fibrinogen, *J Biol Chem 278*, 32251-32258.
15. Delaglio, F., Grzesiek, S., Vuister, G. W., Zhu, G., Pfeifer, J., and Bax, A. (1995) NMRPipe: a multidimensional spectral processing system based on UNIX pipes, *J Biomol NMR 6*, 277-293.
16. Vranken, W., F., Boucher, W., Stevens, T., J., Fogh, R., H., Pajon, A., Llinas, M., Ulrich, E., L., Markley, J., L., Ionides, J., and Laue, E., D. (2005) The CCPN data model for NMR Spectroscopy, *Proteins 59*, 687-696.
17. Vinogradova, O., Velyvis, A., Velyviene, A., Hu, B., Haas, T., Plow, E., and Qin, J. (2002) A structural mechanism of integrin alpha(IIb)beta(3) "inside-out" activation as regulated by its cytoplasmic face, *Cell 110*, 587-597.
18. Rieping, W., Habeck, M., Bardiaux, B., Bernard, A., Malliavin, T. E., and Nilges, M. (2007) ARIA2: automated NOE assignment and data integration in NMR structure calculation, *Bioinformatics 23*, 381-382.
19. Laskowski, R. A., Rullmannn, J. A., MacArthur, M. W., Kaptein, R., and Thornton, J. M. (1996) AQUA and PROCHECK-NMR: programs for checking the quality of protein structures solved by NMR, *J Biomol NMR 8*, 477-486.
20. de Vries, S. J., van Dijk, M., and Bonvin, A. M. (2010) The HADDOCK web server for data-driven biomolecular docking, *Nature protocols 5*, 883-897.
21. Baker, N. A., Sept, D., Joseph, S., Holst, M. J., and McCammon, J. A. (2001) Electrostatics of nanosystems: application to microtubules and the ribosome, *Proc Natl Acad Sci U S A 98*, 10037-10041.
22. Dolinsky, T. J., Czodrowski, P., Li, H., Nielsen, J. E., Jensen, J. H., Klebe, G., and Baker, N. A. (2007) PDB2PQR: expanding and upgrading automated preparation of biomolecular structures for molecular simulations, *Nucleic acids research 35*, W522-525.
23. Pettersen, E. F., Goddard, T. D., Huang, C. C., Couch, G. S., Greenblatt, D. M., Meng, E. C., and Ferrin, T. E. (2004) UCSF Chimera--a visualization system for exploratory research and analysis, *J Comput Chem 25*, 1605-1612.
24. Al-Hashimi, H. M., Valafar, H., Terrell, M., Zartler, E. R., Eidsness, M. K., and Prestegard, J. H. (2000) Variation of molecular alignment as a means of resolving orientational ambiguities in protein structures from dipolar couplings, *J Magn Reson 143*, 402-406.
25. Dosset, P., Hus, J. C., Marion, D., and Blackledge, M. (2001) A novel interactive tool for rigid-body modeling of multi-domain macromolecules using residual dipolar couplings, *J Biomol NMR 20*, 223-231.
26. Gurtovenko, A. A., and Vattulainen, I. (2007) Lipid transmembrane asymmetry and intrinsic membrane potential: two sides of the same coin, *J Am Chem Soc 129*, 5358-5359.

TABLES

Table 1. Statistical Data for NMR Structural Calculations

Total distance constraints	
NOEs	2647
Intra-residue	888
|i-j|=1	701
|i-j|<5	354
|i-j|>4	704
Hydrogen bond constraints	156
Dihedral angle restraints	311
$^1D_{HN}$ RDC restraints	351
RMSD for NMR constraints	
Distance constraints (Å)	0.209 ± 0.014
Dihedral angle restraints (°)	1.428 ± 0.133
RDCs (Hz)	2.317 ± 0.106
Deviations from idealized geometry	
Bonds (Å)	0.012 ± 0.000
Angles (°)	1.460 ± 0.042
Impropers (°)	1.729 ± 0.045
RMSD (Å) for Sk4 domain (residues 1227-1327)	0.97
RMSD (Å) for Sk5 domain (residues 1344-1380, 1391-1427)	1.37
RMSD (Å) for Sk45 tandem (residues 1227-1327, 1344-1427)	3.1
Procheck ramachandran statistics (%)	
most favored regions	65.3
allowed regions	27.3
generously allowed regions	5.6
disallowed regions	1.8

Table 2. Thermodynamic Analysis of the Association of Skelemin and Integrin by ITC

Titrant	C-terminal β_3	N-terminal β_3	α_{IIb}
Protein	Sk4	Sk45	Sk45
Kd (SM)	10.7 ± 9.9	37.2 ± 180	14.2 ± 4.3
ΔG (kJ/mol)	-28.3	-25.3	-27.7
ΔH (kJ/mol)	-0.7 ± 0.1	-1.7 ± 0.9	-1.6 ± 0.1
-TΔS (kJ/mol)	-27.6	-23.6	-26.1
Stoichiometry, n	0.99 ± 0.10	1.30 ± 0.41	1.26 ± 0.05

*Titration of Sk45 with N-terminal β_3 was noisy, resulting in inaccurate fitting.

FIGURES LEGENDS

Figure 1. Sk45 NMR ensemble obtained through the calculation where RDC data for the two domains was used independently (**A-B**). Sk4 domain and N-terminal part of the linker is shown

in orange, Sk5 domain – in blue, the unstructured part of the linker – in green. **A:** The structures are superimposed over the domain 4 of the tandem Sk45 well-ordered residues 1227-1327. **B:** The structures are superimposed over domain 5 of the tandem Sk45 well-ordered residues 1344-1380 and 1391-1427. Additional data used to confirm inter-domains orientation (**C-D**). **C:** The residues affected by the introduction of m-PROXYL spin label are in red. The spin modified residue is shown with the thicker bonds and side chain displayed. **D:** The residues of Sk4 domain and the beginning of linker affected by the presence of the Sk5 domain are shown with thicker bonds. The affected residues were deduced from chemical shift perturbations in ^{1}H-^{15}N HSQC spectra of Sk4 and Sk45 constructs.

Figure 2. The quality of RDCs fits: the correlation fits of the experimental and back-calculated RDCs for the best structure from the NMR ensemble presented in Figure 1. **A:** $^{1}D_{HN}$ RDCs data is split into two parts, one for each domain: data in orange corresponds to Sk4 domain and data in blue – to Sk5 domain. **B:** The correlation fits of the experimental and back-calculated RDCs for the best structure from the NMR ensemble. These fits are obtained for $^{1}D_{HN}$ RDCs used as a single data set for the two domains. The four RDCs fits are (from left to right): Sk45 with His-tag in Pf1 anisotropic medium, Sk45 without tag in Pf1, C12E5/hexanol or C12E5/hexanol/SOS media. The fits are obtained with MODULE (*25*).

Figure 3. The overlay of Sk45 NMR ensemble with the X-ray structure of human homolog (PDB ID 3RBS) and the respective quality of RDCs fits. **A:** The 20 lowest energy NMR structures with the two domains oriented by means of RDC data. The NMR ensemble and the X-ray structure (violet) are superimposed over residues 1227-1327 (domain Sk4) and 1344-1427 (domain Sk5). The linker region is magnified and is shown in ribbon presentation for X-ray structure. **B:** The relative orientation of the alignment tensors for Sk45 with His-tag in Pf1 anisotropic medium (red), for Sk45 without tag in Pf1 (magenta), C12E5/hexanol (grey) or C12E5/hexanol/SOS (blue) anisotropic media. **C:** The correlation fits of the experimental and back-calculated $^{1}D_{HN}$ RDCs for the best structure from the NMR ensemble of Sk45. **D:** The correlation fits of the experimental and back-calculated $^{1}D_{HN}$ RDCs for the X-ray structure. The fits are obtained with Xplor-NIH tools.

Figure 4. A: ITC data for the Sk45 interaction with α_{IIb} fitted with a single binding site model. **B:** The NMR ensemble of α_{IIb} cytoplasmic tail in the bound conformation as determined from trNOE data. The conformer used for docking is shown in green. **C:** A region of the ^{1}H-^{15}N HSQC spectra of Sk45 in absence (black) and presence of β_3 (red) at the protein:peptide ratio 1:3. Affected residues are labeled. **D:** Effect of skelemin-derived peptide on $\alpha_{IIb}\beta_3$-expressing CHO cell adhesion. Microtiter wells were coated with 2.5Sg/ml of fibrinogen and postcoated with 1% BSA. Calcein-labeled $\alpha_{IIb}\beta_3$-expressing CHO cells were incubated with different concentration of THIVWYKDEREISVDEKHD (●) or control EREISAAAKHD (○) peptides for 20 min at 22ºC. After 30 min at 37ºC, nonadherent cells were removed, and adhesion was determined. Data points are expressed as a percentage of control adhesion (in the absence of peptides) and are the mean of three individual experiments performed with triplicate determinations in each experiment.

Figure 5. A: Model of tertiary integrin/skelemin complex: Sk45 (tan) is shown bound to cytoplasmic tails of α_{IIb} (green) and β_3 (purple) in ribbon presentation. Key residues are labeled. The inset shows a slightly rotated display of the hydrogen bonding network for a better view. **B:** Zoomed view of the binding interface with Sk5. The surface of Sk5 is colored based on its electrostatic potential. **C:** The tertiary complex is arbitrarily placed with respect to the lipid bilayer represented by POPC and POPE mixture (*26*) shown in gray. Each side is shown to better visualize the binding pockets and potential orientation with the lipid bilayer. The inset depicts Sk5 potentially positively charged residues (colored in blue) that may interact with the lipid bilayer.

For Table of Contents Use Only

Skelemin Association with $\alpha_{IIb}\beta_3$ Integrin: A Structural Model

Vitaliy Gorbatyuk, Khiem Nguyen, Nataly P. Podolnikova, Lalit Deshmukh[+], Xiaochen Lin, Tatiana P. Ugarova and Olga Vinogradova

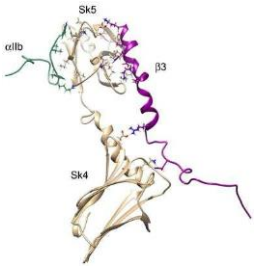

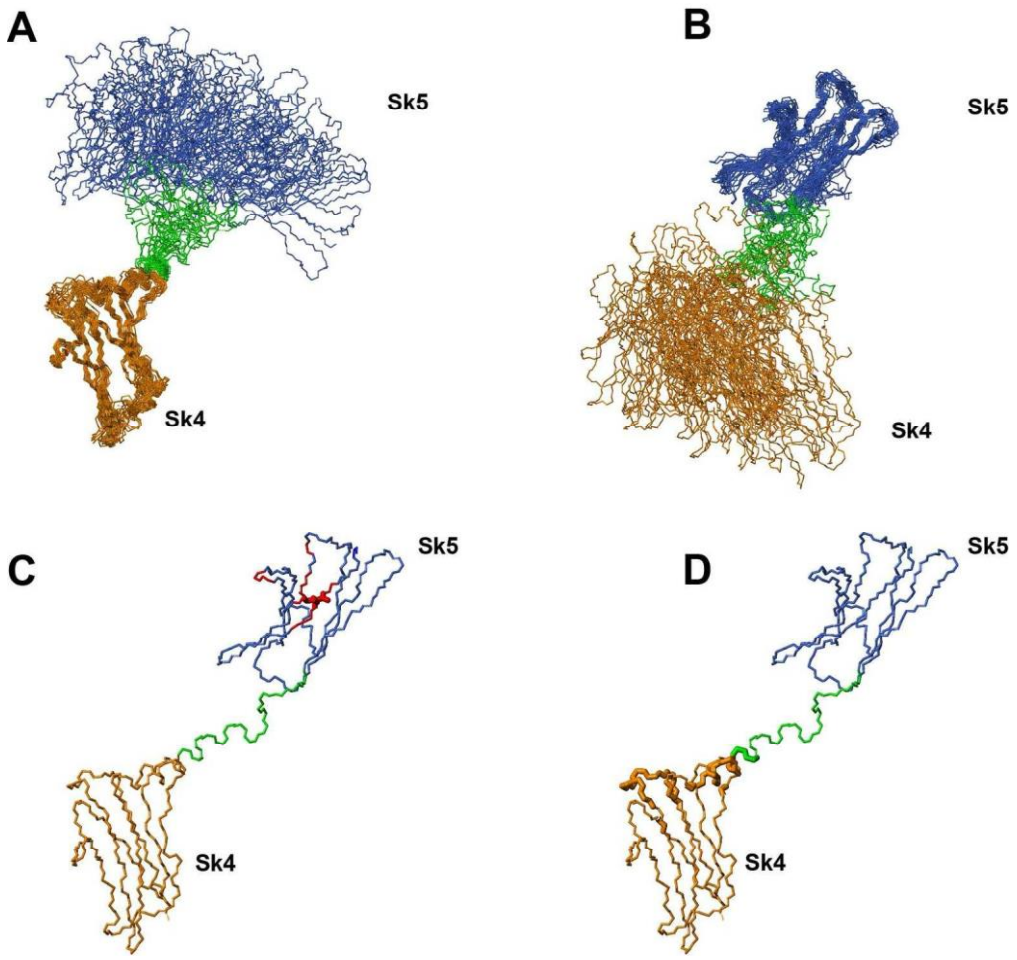

Figure 1. Sk45 NMR ensemble obtained through the calculation where RDC data for the two domains was used independently (A-B). Sk4 domain and N-terminal part of the linker is shown in orange, Sk5 domain – in blue, the unstructured part of the linker – in green. A: The structures are superimposed over the domain 4 of the tandem Sk45 well-ordered residues 1227-1327. B: The structures are superimposed over domain 5 of the tandem Sk45 well-ordered residues 1344-1380 and 1391-1427. Additional data used to confirm inter-domains orientation (C-D). C: The residues affected by the introduction of m-PROXYL spin label are in red. The spin modified residue is shown with the thicker bonds and side chain displayed. D: The residues of Sk4 domain and the beginning of linker affected by the presence of the Sk5 domain are shown with thicker bonds. The affected residues were deduced from chemical shift perturbations in 1H-15N HSQC spectra of Sk4 and Sk45 constructs.
152x144mm (300 x 300 DPI)

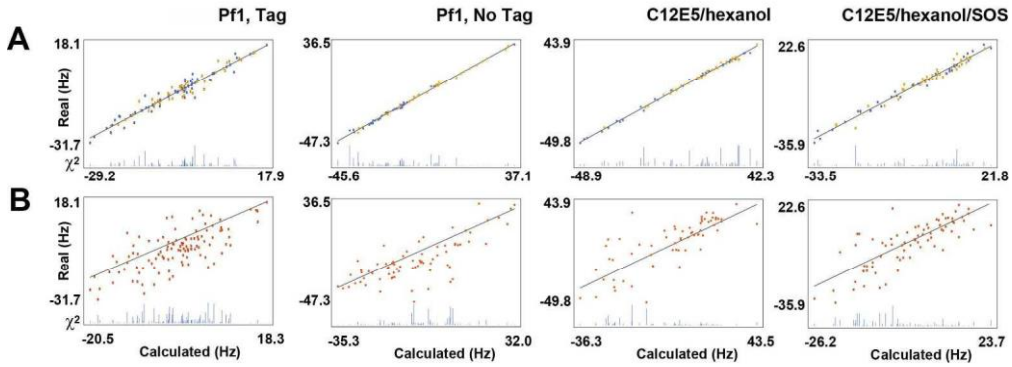

Figure 2. The quality of RDCs fits: the correlation fits of the experimental and back-calculated RDCs for the best structure from the NMR ensemble presented in Figure 1. A: 1DHN RDCs data is split into two parts, one for each domain: data in orange corresponds to Sk4 domain and data in blue – to Sk5 domain. B: The correlation fits of the experimental and back-calculated RDCs for the best structure from the NMR ensemble. These fits are obtained for 1DHN RDCs used as a single data set for the two domains. The four RDCs fits are (from left to right): Sk45 with His-tag in Pf1 anisotropic medium, Sk45 without tag in Pf1, C12E5/hexanol or C12E5/hexanol/SOS media. The fits are obtained with MODULE (25). 201x76mm (300 x 300 DPI)

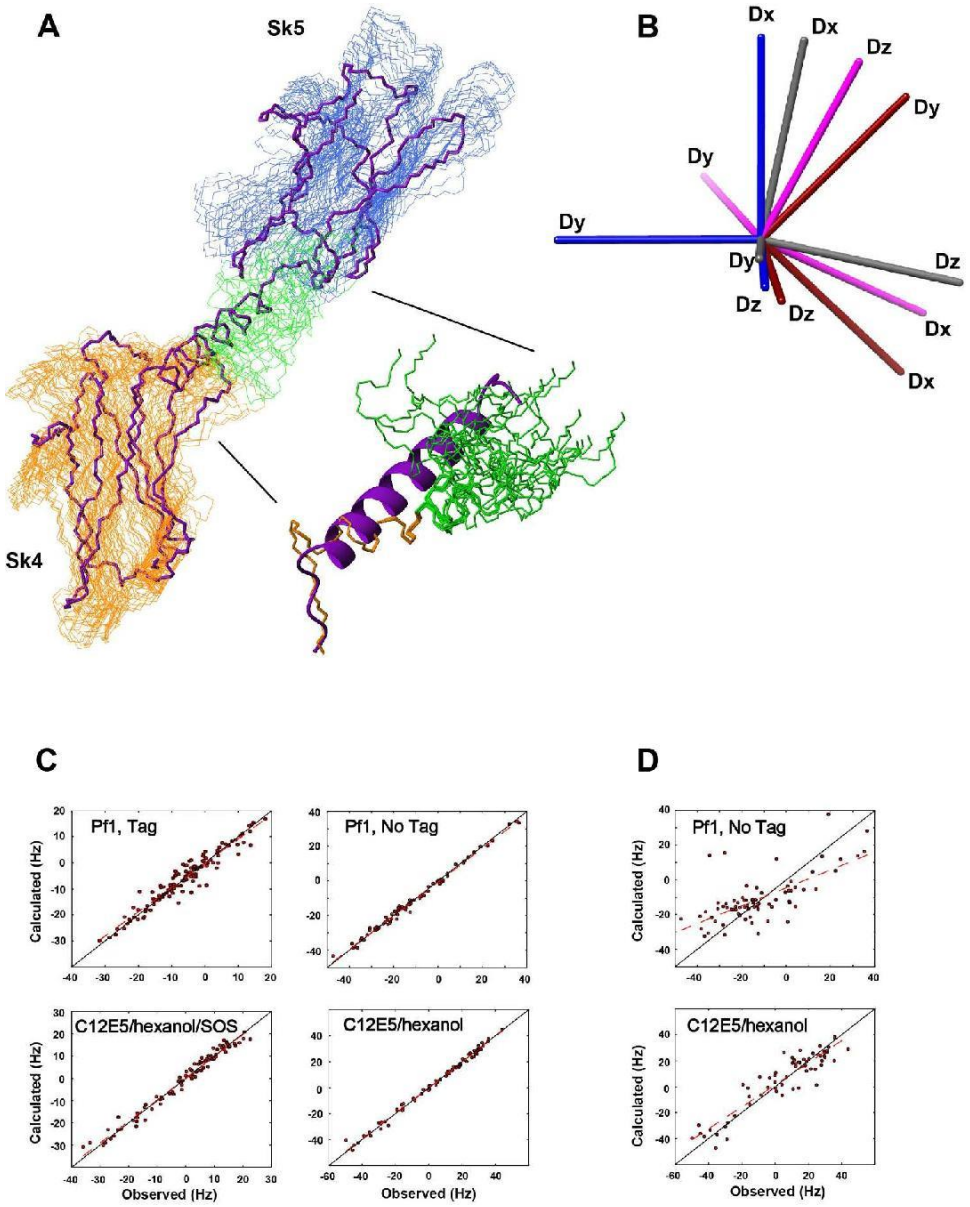

Figure 3. The overlay of Sk45 NMR ensemble with the X-ray structure of human homolog (PDB ID 3RBS) and the respective quality of RDCs fits. A: The 20 lowest energy NMR structures with the two domains oriented by means of RDC data. The NMR ensemble and the X-ray structure (violet) are superimposed over residues 1227-1327 (domain Sk4) and 1344-1427 (domain Sk5). The linker region is magnified and is shown in ribbon presentation for X-ray structure. B: The relative orientation of the alignment tensors for Sk45 with His-tag in Pf1 anisotropic medium (red), for Sk45 without tag in Pf1 (magenta), C12E5/hexanol (grey) or C12E5/hexanol/SOS (blue) anisotropic media. C: The correlation fits of the experimental and back-calculated 1DHN RDCs for the best structure from the NMR ensemble of Sk45. D: The correlation fits of the experimental and back-calculated 1DHN RDCs for the X-ray structure. The fits are obtained with Xplor-NIH tools.
198x240mm (300 x 300 DPI)

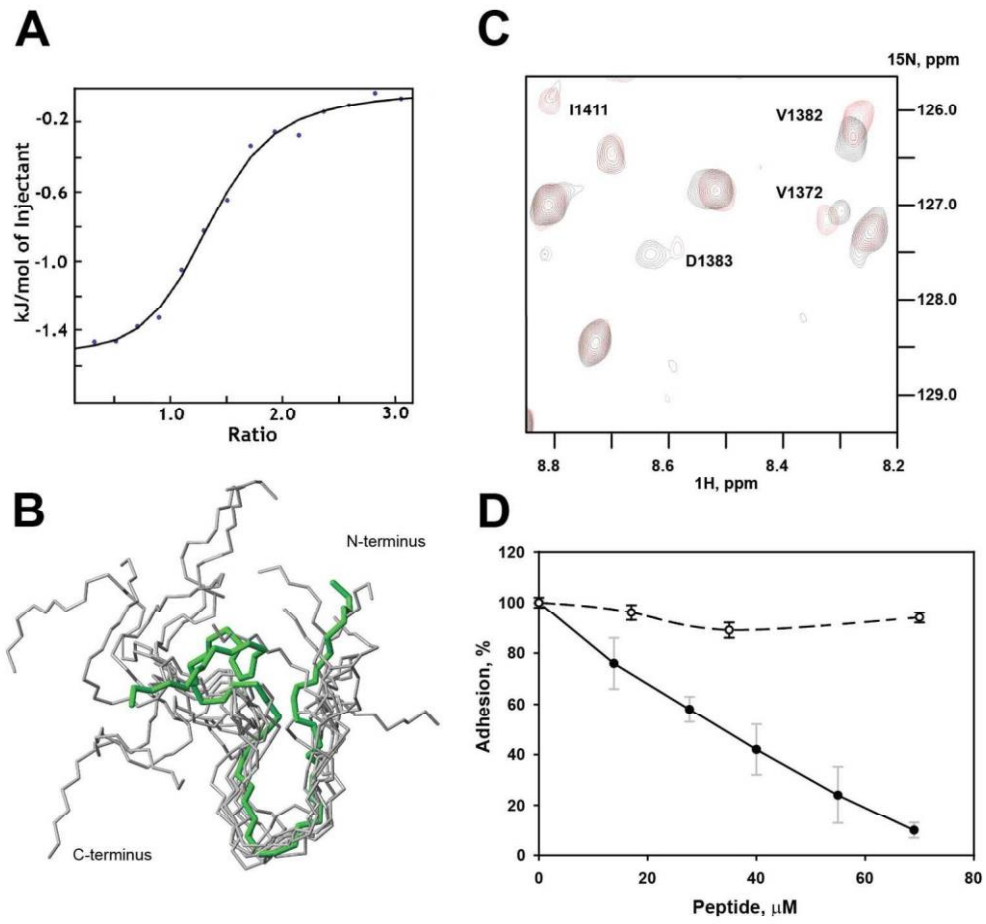

Figure 4. ITC data for the Sk45 interaction with αIIb fitted with a single binding site model. B: The NMR ensemble of αIIb cytoplasmic tail in the bound conformation as determined from trNOE data. The conformer used for docking is shown in green. C: A region of the 1H-15N HSQC spectra of Sk45 in absence (black) and presence of β3 (red) at the protein:peptide ratio 1:3. Affected residues are labeled. D: Effect of skelemin-derived peptide on αIIbβ3-expressing CHO cell adhesion. Microtiter wells were coated with 2.5μg/ml of fibrinogen and postcoated with 1% BSA. Calcein-labeled αIIbβ3-expressing CHO cells were incubated with different concentration of THIVWYKDEREISVDEKHD (●) or control EREISAAAKHD (○) peptides for 20 min at 22ºC. After 30 min at 37ºC, nonadherent cells were removed, and adhesion was determined. Data points are expressed as a percentage of control adhesion (in the absence of peptides) and are the mean of three individual experiments performed with triplicate determinations in each experiment. 131x132mm (300 x 300 DPI)

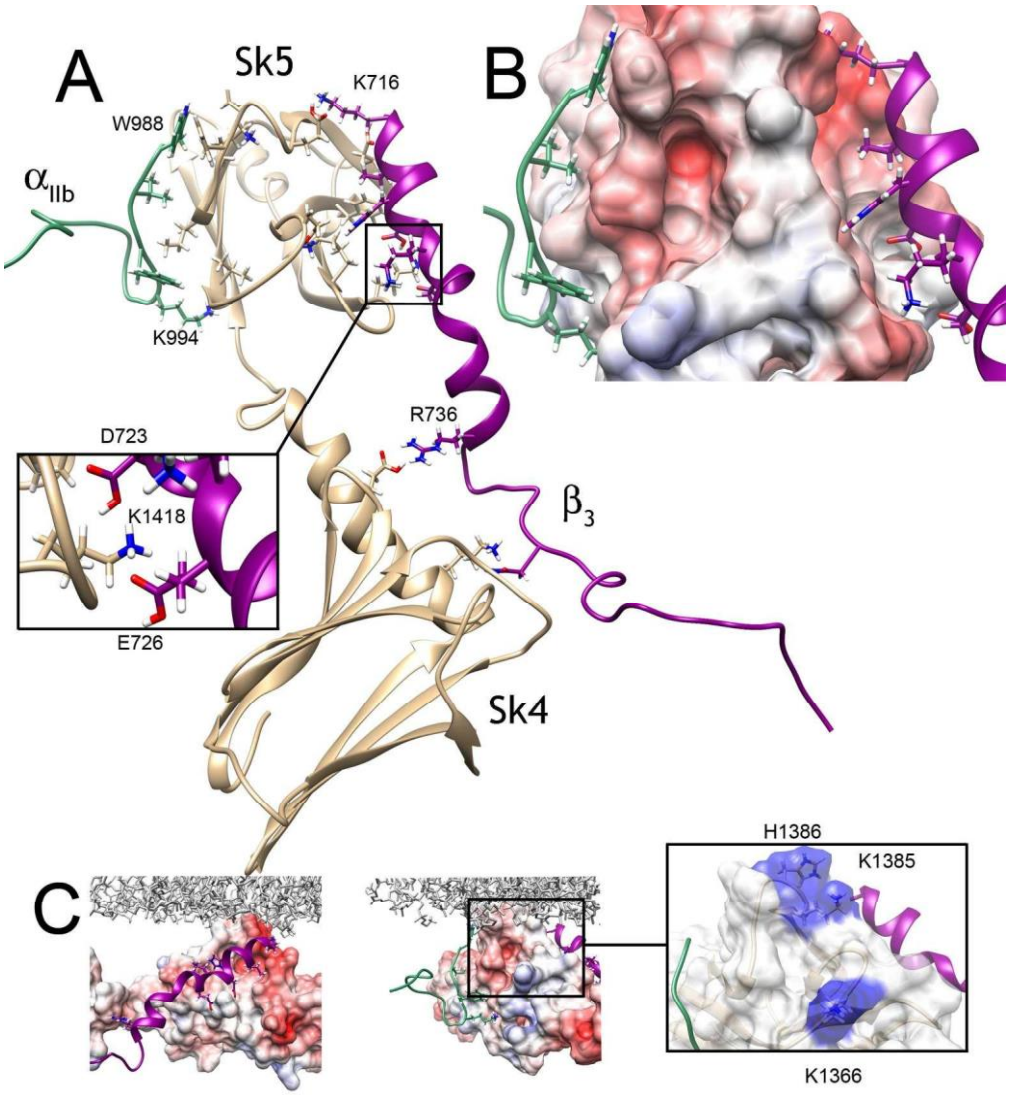

Figure 5. Model of tertiary integrin/skelemin complex: Sk45 (tan) is shown bound to cytoplasmic tails of αIIb (green) and β3 (purple) in ribbon presentation. Key residues are labeled. The inset shows a slightly rotated display of the hydrogen bonding network for a better view. B: Zoomed view of the binding interface with Sk5. The surface of Sk5 is colored based on its electrostatic potential. C: The tertiary complex is arbitrarily placed with respect to the lipid bilayer represented by POPC and POPE mixture (26) shown in gray. Each side is shown to better visualize the binding pockets and potential orientation with the lipid bilayer. The inset depicts Sk5 potentially positively charged residues (colored in blue) that may interact with the lipid bilayer.
177x194mm (300 x 300 DPI)